JOURNAL OF MATERIALS SCIENCE 29 (1994) 3295–3308

Measurement and theory of the orientation dependence of Knoop microhardness in single-crystal mercuric iodide

J. MARSCHALL*, F. MILSTEIN
Departments of Materials and Mechanical Engineering, University of California, Santa Barbara, CA 93106, USA

Measurements were made of the orientation dependence of the Knoop microhardness H_K on the (0 0 1) and (1 1 0) faces of single crystals of red (tetragonal) mercuric iodide that were vapour-grown for use in radiation detectors. The (0 0 1) faces of the crystals are softest when the major diagonal of the Knoop indentor (called here "the indentor") is parallel to the [1 0 0] crystallographic axis, and H_K increases monotonically, by about 25%, as the indentor is rotated from the [1 0 0] to the [1 1 0] axis. The (1 1 0) surfaces are hardest when the indentor is parallel to [0 0 1]; H_K decreases by about 50% as the indentor is rotated from [0 0 1] to [1 $\bar{1}$ 0]; the experimental data indicate an intermediate microhardness minimum that occurs before the [1 $\bar{1}$ 0] orientation is reached. Particularly interesting surface topography, including bands of slip lines, is observed in the vicinity of indentations on the (1 1 0) planes, which apparently have not previously been characterized by Knoop microhardness indentation. Theoretically, the size of a microhardness indention is presumed to depend on the volume of material in which appropriate slip systems are stressed sufficiently to cause appreciable slip. To test this concept and determine which particular slip systems dominate the indention process, the "infinite flat punch" model was used to calculate the orientational and volumetric variations of shear stress on various potential slip systems in mercuric iodide. For indention processes controlled by movement (i.e. slip) of material in the [0 0 1] direction, over {1 0 0} planes, these calculations predict the following (experimentally observed) results: (a) on the (0 0 1) plane, H_K is smallest at [0 0 1] and greatest at [1 1 0], with no intermediate extremum; (b) on the (1 1 0) plane, H_K has its greatest value at [0 0 1] and a minimum between [0 0 1] and [1 $\bar{1}$ 0]; (c) H_K at [1 1 0] on the (0 0 1) plane is essentially the same as H_K at [1 $\bar{1}$ 0] on the (1 1 0) plane; and (d) the relative variation of H_K is greater on the (1 1 0) than on the (0 0 1) surface. Finally, the expected orientational variation of H_K on the (1 0 0) and (1 0 1) surfaces was determined theoretically.

1. Introduction

Mercuric iodide (HgI_2) is a wide band-gap, high atomic mass semiconductor which finds application as a room-temperature detector material for γ-ray, X-ray and visible radiation. The room-temperature red phase of HgI_2 crystallizes in a layered structure, with monoatomic planes of iodine and mercury atoms stacked perpendicular to the [0 0 1] (or c) axis in the sequence ... IHgIIHgIIHgI ... . Red HgI_2 has a tetragonal unit cell with lattice constants $a = 0.4356$ nm and $c = 1.234$ nm; the basis consists of two mercury atoms at the positions $\{0,0,0\}$ and $\{1/2,1/2,1/2\}$ and four iodine atoms at $\{0,1/2,u\}$, $\{1/2,0,\bar{u}\}$, $\{0,1/2,u+1/2\}$, and $\{1/2,0,1/2-u\}$, where $u = 0.14$ [1]. Each mercury atom is covalently bonded to two iodine atoms in the layer below and two iodine atoms in the layer above; bonding between adjacent iodine layers is van der Waals in nature.

The plastic deformation characteristics of red HgI_2 strongly reflect this layered crystal structure. As demonstrated by James and Milstein [2] in a series of compression tests of HgI_2 single crystals in various orientations, bulk plastic deformation at room temperature proceeds solely by slip over (0 0 1) (or c) planes; crystals oriented in such a fashion that the resolved shear stress on (0 0 1) planes was zero failed by brittle fracture or by buckling. Slip over (0 0 1) planes has been termed "easy glide" slip. Dislocations that are mobile during easy-glide slip lie with their dislocation lines and Burgers vectors parallel to (0 0 1) planes and are termed easy-glide dislocations. Etching [3–5] and X-ray topographic studies [6] have revealed dislocations whose cores (dislocation lines) intersect (0 0 1) planes. Such dislocations are labelled "hard glide" dislocations because they are essentially immobile under uniformly applied compressive stresses [2]. However, the large, highly localized shear stresses that are produced in a microhardness test can cause appreciable movement of hard-glide dislocations (or hard-glide slip) [4, 5].

* *Present address*: NASA Ames Research Center, Mail Stop 234-1, Moffett Field CA 94035, USA.

0022–2461

Here we report both measurements of Knoop microhardness in HgI_2 and computations of stress distributions on hard-glide slip systems. Comparison of our experimental and theoretical results enables us to determine which specific slip systems dominate the indentation process and how slip on these systems controls the orientation dependence of Knoop microhardness in HgI_2. Several previous studies [4, 5, 7–11] have employed Knoop microhardness testing on (0 0 1) surfaces of single crystal HgI_2 for purposes of material characterization. James and Milstein [4] used an etchant consisting of 5% ethanol in 95% trichloroethylene (TCE) to demonstrate that Knoop microhardness indentations made on (0 0 1) surfaces can induce linear dislocation arrays which emanate, from the indention, in ⟨1 0 0⟩ directions. The etch pits were square and did not change substantially, either in location or shape, with repeated etching. It was deduced that the dislocations corresponding to these etch pits lie with their cores (dislocation lines) parallel to {1 0 0} planes and perpendicular to the (0 0 1) surface. In a later study [5], in which various indentor loads (from 1 to 50 g) were used, etching revealed induced dislocations at most indentations; the higher the load, the greater the number and length of the emanating arrays. It was found that a critical load of 2–5 g was necessary for any significant array development. A series of 10 g Knoop microhardness tests, conducted at various temperatures between 20 and 120 °C, showed that while the array lengths increased substantially with increasing temperature, the Knoop microhardness number H_K remained approximately constant.

It was shown by Milstein *et al.* [8] that extended dislocation arrays are not always found at hardness indentations. They tested three types of microstructurally distinct (0 0 1) surfaces, characterized by either (i) a relative lack of etch pits, (ii) a high density of random etch pits, or (iii) orthogonal etch pit arrays aligned with ⟨1 0 0⟩ directions. The etching of hardness indentations in areas relatively free of etch pits revealed few induced dislocations and no extended arrays. The regions containing ingrown orthogonal dislocation arrays were the hardest of all and those with a high density of random etch pits were the softest. The regions free of etch pits tended to be brittle; cracking along ⟨1 0 0⟩ directions was most evident in these regions and was observed to occur more frequently as the long indentor diagonal was rotated from ⟨1 1 0⟩ to ⟨1 0 0⟩.

Vapour-grown HgI_2 single crystals, used for detector fabrication, are not generally homogeneous; distinct regions of differing defect density form during the growth process. These regions are roughly distinguished by their optical clarity as "hazy" or "clear" [11]. Hazy regions have a significantly higher density of ⟨1 0 0⟩ oriented, rod-like, defects than clear regions and show much more etch pitting after potassium iodide (KI)–H_2O or ethanol–TCE etches. Knoop microhardness testing on large (0 0 1) faces of crystal centre slices with both hazy and clear regions showed the hazy regions to be softer and more ductile than the clear regions [11]. Measurements were made with the long diagonal of the Knoop indentor aligned parallel to either the ⟨1 0 0⟩ or ⟨1 1 0⟩ directions; the results are summarized in Table I. For any given indentor orientation the average value of H_K for these specimens is greater in the clear regions than in the hazy regions. These hardness variations presumably arise because of differences in the defect density and microstructure of the different crystal regions. Of equal note is the observation that for any given specimen and any given region (i.e. clear or hazy) the average value of H_K is always greater when the indentor is aligned in the ⟨1 1 0⟩ direction. This hardness variation apparently relates more directly to the intrinsic slip systems which operate in HgI_2 single crystals.

TABLE I Average Knoop microhardness H_K on the (0 0 1) surfaces of three HgI_2 single crystal specimens, in optically hazy and clear regions, with the major axis of the indentor aligned either with the [1 0 0] or with the [1 1 0] crystal axes; the number of measurements taken for each average value of H_K is shown in brackets and the standard deviation is also given

Crystal specimen	Indentor orientation	H_K	
		Hazy region	Clear region
N1-18	[1 0 0]	11.6 ± 0.6 (31)	15.2 ± 1.4 (84)
	[1 1 0]	13.9 ± 0.8 (89)	17.4 ± 1.5 (46)
N11-18	[1 0 0]	11.5 ± 1.4 (47)	18.2 ± 2.8 (26)
	[1 1 0]	14.1 ± 1.1 (118)	24.3 ± 2.5 (35)
V4-11	[1 0 0]	10.5 ± 0.9 (82)	11.9 ± 1.6 (46)
	[1 1 0]	13.3 ± 1.2 (59)	19.5 ± 2.1 (16)

The present paper examines the orientation dependence of Knoop microhardness in single-crystal HgI_2, both experimentally and theoretically. In particular, we report new measurements of the Knoop microhardness on the (0 0 1) and {1 1 0} crystallographic faces of HgI_2, taken at various indentor orientations, ranging from ⟨1 0 0⟩ to ⟨1 1 0⟩ on the (0 0 1) planes and from [0 0 1] to ⟨1 1 0⟩ on the {1 1 0} planes. Theoretically, we adopt the viewpoint that the size of a microhardness indentation will depend upon the volume of the crystal, in the vicinity of the indentor, throughout which the shear stress on potential hard-glide slip systems exceeds the critical resolved shear stress (CRSS) for these systems. In order to test this concept and to determine which particular slip systems control the indentation size, the infinite flat punch (IFP) model [12] is used to calculate the orientational and volumetric variations of the shear stress on the various HgI_2 slip systems proposed by Georgeson and Milstein [13]. It is found that these variations of shear stress on the {1 0 0} [0 0 1] hard-glide slip systems correspond remarkably well with all of the experimental results. That is, for both the (0 0 1) and (1 1 0) planes of HgI_2, the decreases (or increases) in Knoop microhardness, observed when the indentor orientation is changed, can be directly correlated with increases (or decreases) in the relative volume of material stressed past a prescribed CRSS on the {1 0 0} [0 0 1] slip systems (as calculated with the IFP model).

2. Experimental procedure and results

The HgI_2 specimens used for the present study were supplied by EG&G Energy Measurements Inc., Santa Barbara Operations, USA, in the form of 2–4 mm thick slabs which had been solution sawn from vapour-grown single crystals and polished in a KI–H_2O solution to produce two flat and parallel faces. Microhardness measurements on (0 0 1) surfaces were performed on both clear and hazy test specimens (from crystal V5-13), while – due to limited specimen availability – tests on {1 1 0} surfaces were done on hazy specimens (from crystal N13-21) only. The measurements were made using a Tukon microhardness tester that was fit with a rotary stage inscribed at 2° increments. The orientations of the long Knoop indentor diagonal, relative to specific crystallographic directions in the plane of the specimen surface, were determined optically in the following way. For (0 0 1) surfaces, the ⟨1 0 0⟩ directions were established by the orientation of ingrown rod-like defects which are aligned with ⟨1 0 0⟩ directions and can be clearly resolved using transmitted-light optical microscopy; alignment was also verified by cleavage steps that form along ⟨1 0 0⟩ directions. For the case of {1 1 0} surfaces, ⟨1 1 0⟩ directions were oriented by finding the perpendicular intersection of (0 0 1) cleavage planes with the surface. This was done by using masking tape to remove small flakes of material from one of the side faces of the specimen; these flakes cleave cleanly on (0 0 1) planes, producing a sharp intersection with the test surface. Additionally, ⟨1 1 0⟩ directions were confirmed by the linear slip lines which were induced on {1 1 0} surfaces by Knoop indentations (as discussed below). The initial alignment error, between the long indentor diagonal and a crystallographic direction deduced by the above procedures, is estimated at $\pm 3°$. Photomicrographs were taken using a Nikon Labophot Metallurgical microscope with a Microflex AFX-II camera attachment.

Knoop microhardness numbers were calculated from the usual formula (i.e. $H_K = 0.014228\ P/d^2$), using the known test load P (g) and the measured length of the long diagonal of the residual indentation d (mm). In a previous study [5], the load dependence of the Knoop microhardness was investigated in the range of 1 to 50 g on successively cleaved (0 0 1) surfaces of a particular HgI_2 crystal; H_K was found to decrease with increasing load from a high of 35.5 at 1 g to a low of 14.7 at 50 g, although H_K was fairly insensitive to load in the range of 5 g ($H_K = 18.5$) to 25 g ($H_K = 17.2$); a 10 g test load was adopted as standard. These tests were carried out with the major axis of the indentor aligned with ⟨1 1 0⟩ directions. We have similarly examined the influence of load variation for two indentor orientations on the (1 1 0) planes. The results of these tests are shown in Table II. Although the observed variation of H_K with load on the (1 1 0) plane is somewhat greater than that found on the (0 0 1) plane, for the indentations on the (1 1 0) plane the ratio $H_{K[1\bar{1}0]}/H_{K[001]}$ is very close to a constant value (of about 0.47) in the range of $P = 10$ to 50 g. Thus the relative variation of microhardness apparently is independent of load in this range. (The meaning of $H_{K[hkl]}$ is explained in Table II). In order to facilitate comparison among the various tests, a 10 g indentor load was also selected as the standard load for the present determinations of the orientation dependence of Knoop microhardness in HgI_2.

TABLE II Average Knoop microhardness $H_{K[hkl]}$ on the (1 1 0) surface of HgI_2 under various loads of indentation P, where the subscripts $[hkl]$ indicate the crystal axes to which the long diagonal of the indentor is parallel; each value is the average of at least 10 tests; and the standard deviations are given

P (g)	$H_{K[0\,0\,1]}$	$H_{K[1\,\bar{1}\,0]}$
5	29.0 ± 3.6	20.0 ± 1.8
10	28.6 ± 1.9	13.5 ± 2.3
25	24.8 ± 1.5	11.2 ± 2.5
50	22.3 ± 1.4	10.9 ± 1.6

Fig. 1a and b illustrate the indentor orientations for the microhardness measurements made on the (0 0 1) and (1 1 0) planes, respectively. For tests conducted on (0 0 1) planes, the orientation angle θ is taken as 0° when the long diagonal of the indentor is aligned with the [1 0 0] direction and θ is 45° when the long diagonal is parallel to [1 1 0]; for tests on (1 1 0) planes θ is taken as 0° when the long indentor diagonal is aligned with the [0 0 1] direction and θ is equal to 90° when it is parallel to $[1\,\bar{1}\,0]$.

Fig. 2 shows the orientational dependence of Knoop microhardness measured on the (0 0 1) surfaces of both hazy and clear HgI_2 test specimens. Each datum point is the average of twenty measurements and the standard deviation from the average is shown by the error bars. The results plotted in Fig. 2 show that the average values of the microhardness increase by about 30% in the clear regions of the crystal and by about 25% in the hazy regions, as the orientation angle is changed from 0 to 45°. These changes are comparable to those observed in the crystals listed in Table I. The data are generally consistent with H_K increasing monotonically as θ varies from 0° to 45°. The findings reported by James *et al.* [11], that hazy regions are generally softer than clear regions, are shown in the present work to be independent of test orientation; i.e. at each indentor orientation the average microhardness is greater in the clear regions than in the hazy regions. Examples of Knoop indentations on a (0 0 1) surface of a single-crystal HgI_2 specimen are shown in Fig. 3. This photomicrograph is of a hazy region of the crystal, observed in transmitted light. The rod-like defects are clearly visible and the indentation oriented parallel to these defects (i.e. along the [1 0 0] direction) is noticeably longer than the indentation aligned with the [1 1 0] direction.

Previous studies of Knoop microhardness indentations upon (0 0 1) surfaces have focused upon the development of linear dislocation arrays which have often been found to emanate from the indentation along ⟨1 0 0⟩ directions. Such arrays have been observed as etch pits by optical microscopy [4, 5, 8] and as dark cross patterns during cathodoluminescence electron microscopy [8–10]. In the present work, repeated ethanol–TCE etches of both hazy and clear test specimens did not reveal any such extended arrays.

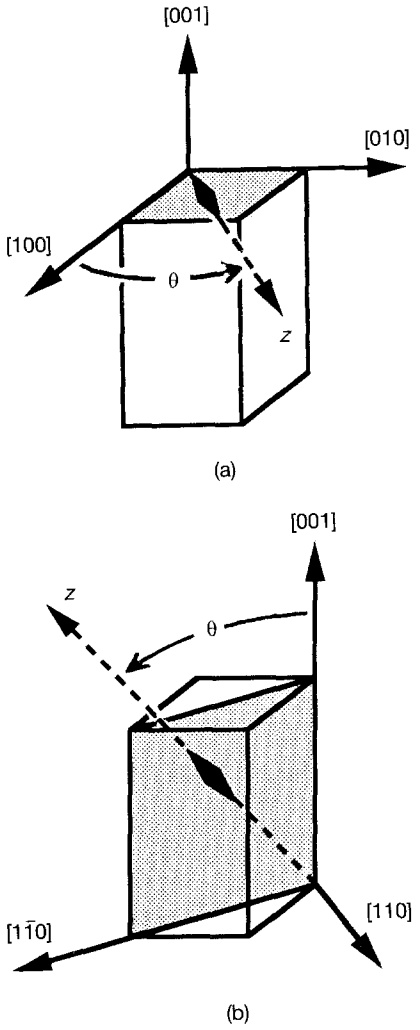

Figure 1 Illustration of indentor orientation and definition of orientation angle θ for microhardness measurements made on (a) (0 0 1) surfaces and (b) (1 1 0) surfaces of single-crystal HgI_2. In each case the crystal surface that is tested is shown shaded. The z axis lies in the test surface and is coincident with the long diagonal of the indentor.

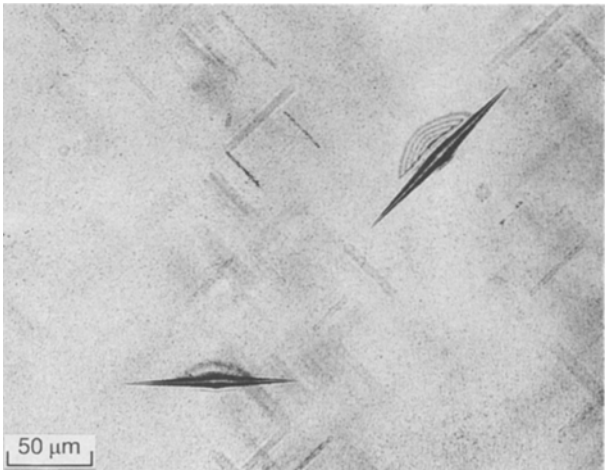

Figure 3 Knoop microhardness indentations on the (0 0 1) plane of hazy single-crystal HgI_2, observed in transmitted light. The rod-like defects are aligned with ⟨1 0 0⟩ crystallographic directions.

Only a comparatively small number of etch pits in the immediate vicinity of the indentations were seen; similar observations were made by Milstein *et al.* [8] for surfaces relatively free of background etch pits.

The variation of H_K with indentor orientation on (1 1 0) planes is shown in Fig. 4. Again, each datum point is the average of twenty measurements and the standard deviations are indicated by the error bars. As the indentor is rotated from a [0 0 1] to a [1 $\bar{1}$ 0] alignment, the value of H_K falls by about half. This decrease in microhardness is most rapid in the range of $\theta \simeq 15$–$40°$, during which approximately 50% of the total change takes place. The average Knoop microhardness exhibits a minimum at around 75°. A monotonic dependence of H_K upon θ in the range 0 to 90° is also consistent (within experimental deviation) with the data, although there is a theoretical basis for the intermediate Knoop microhardness minimum, as explained below in Section 3.2.

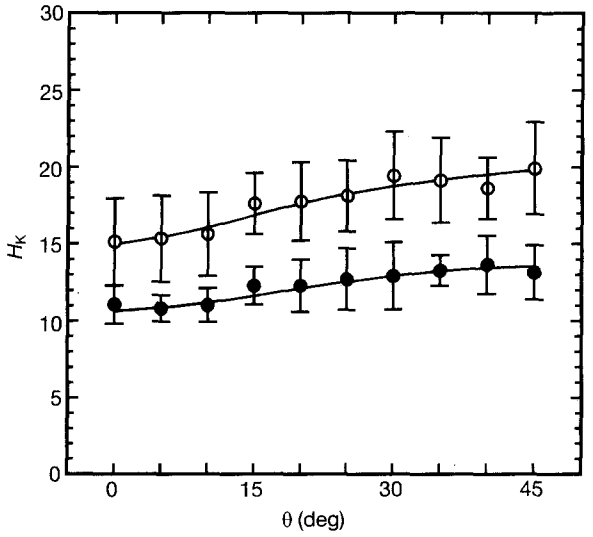

Figure 2 Results of measurements of Knoop microhardness as a function of indentor orientation angle θ for indentations made on the (0 0 1) planes of (●) hazy and (○) clear regions of single-crystal HgI_2; θ is the angle between the [1 0 0] crystallographic axis and the long diagonal of the Knoop indentor.

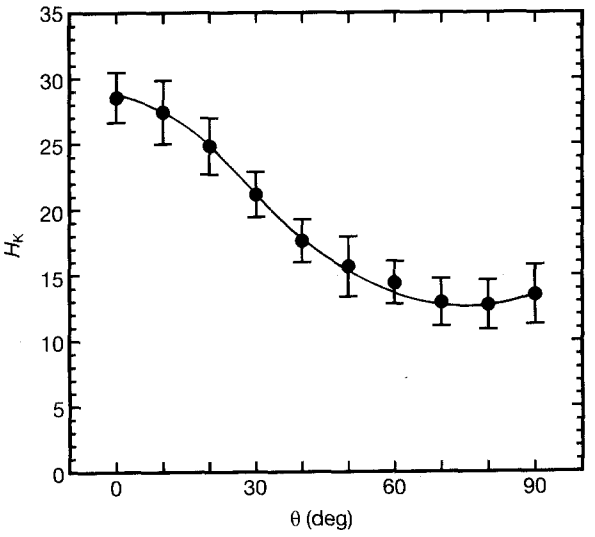

Figure 4 Results of measurements of the dependence of Knoop microhardness upon indentor orientation angle θ for indentations made on the (1 1 0) planes of hazy regions of single-crystal HgI_2; θ is the angle between the [0 0 1] crystallographic axis and the long diagonal of the Knoop indentor.

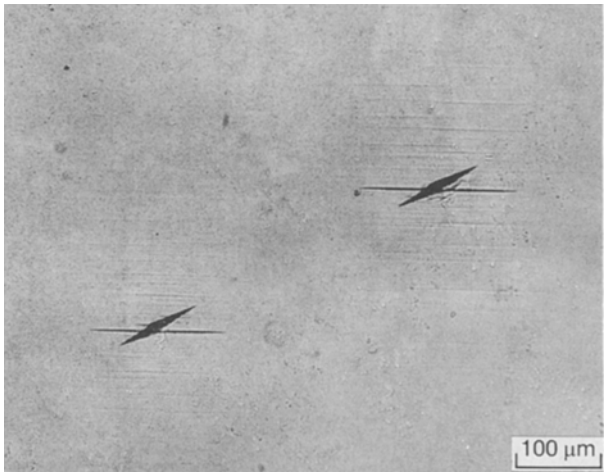

Figure 5 Examples of Knoop microhardness indentations made at $\theta \simeq 60°$ on the (1 1 0) plane of single-crystal HgI_2, observed in transmitted light. Horizontal slip lines in the vicinity of the indentations (and a crack protruding from each indentation) are parallel to the [1 $\bar{1}$ 0] direction.

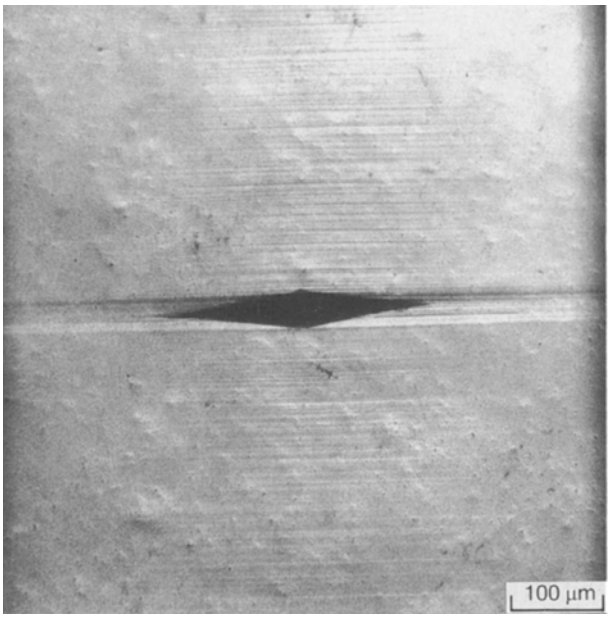

Figure 7 Knoop microhardness indentation on the (1 1 0) plane of single-crystal HgI_2 at $\theta \simeq 90°$, observed in reflected light.

Photomicrographs of Knoop microhardness indentations made on the (1 1 0) surface, at various indentor orientation angles, are shown in Figs 5–7. These figures exhibit a prominent topographical feature common to all of the indentations on the (1 1 0) surfaces, i.e. the surface is scored with a band of closely spaced lines parallel to the [1 $\bar{1}$ 0] direction. The band of slip lines occurs in regions adjacent to the Knoop impression and extends along the [0 0 1] direction. These lines are interpreted as resulting from slip of material into the bulk on (0 0 1) planes. Similar observations have been reported for Vickers indentations on the (1 0 0) plane of the layered crystal BaFCl [14]. In the present study, the number and discernible length of these lines, as well as the size of the regions in which they are evident, increases as the indentor orientation is rotated from 0 to 90°. When the long diagonal of the Knoop indentor is aligned parallel to the [1 $\bar{1}$ 0] direction, the resulting indentations lie within a groove of material that has been depressed below the ambient surface, as is seen (under reflected light) in the photomicrograph of Fig. 7. (In order to highlight this effect, a 50 g load was used to make the indention shown in this particular photomicrograph.) The groove is

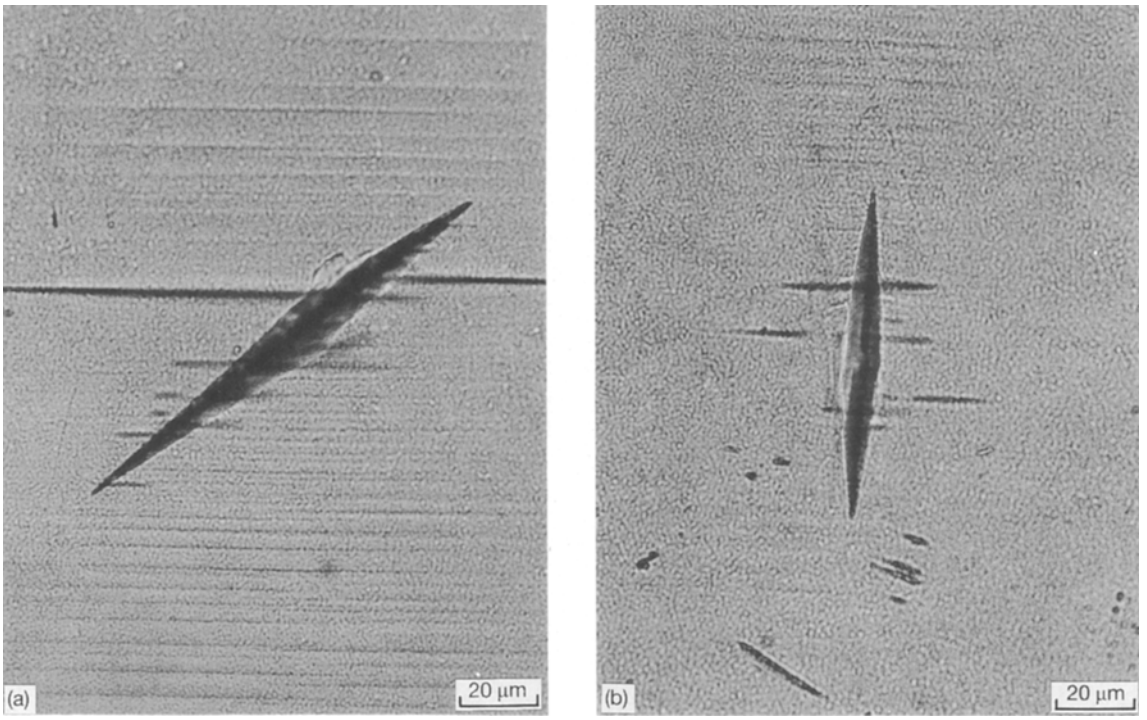

Figure 6 Knoop microhardness indentations on the (1 1 0) plane of single-crystal HgI_2 observed in transmitted light: (a) $\theta \simeq 55°$, (b) $\theta \simeq 0°$. The horizontal slip lines are parallel to [1 $\bar{1}$ 0].

deepest at the indentation and gradually becomes shallower as the distance from the indentation increases along [1 $\bar{1}$ 0] directions; when a standard 10 g indention load is used, the groove merges back into the ambient surface at about 200–400 μm from the centre of the indentation.

Indentions on the (1 1 0) surface also often caused cracks parallel to [1 $\bar{1}$ 0] to appear. This type of fracture is not unexpected since HgI_2 crystals cleave quite readily between (0 0 1) planes, due to the weak bonding between adjacent iodine layers. Such cracks were most pronounced at intermediate indentor angles (i.e. 20–70°); generally, for such indentions, a single major and several minor cracks were induced by the indentor, as is evident in Figs 5 and 6a. The major crack usually originated near the centre of the impression and extended about one indentation length from it. As θ approached 0° only a few smaller cracks were observed, as is seen in Fig. 6b.

3. Theory

This section presents our theoretical computations of shear stress on expected slip systems, for correlation with our experimental microhardness measurements. Potential slip systems in HgI_2 have been categorized as types 1–6 by Georgeson and Milstein [13] and are listed in Table III and illustrated in Fig. 8. We begin by reviewing the likely ordering of the critical resolved shear stresses required to initiate appreciable slip on these systems. In Fig. 8, each type of slip system is characterized by a dislocation loop acting on the slip plane and by an arrow indicating the direction of the Burgers vector (i.e. the direction of slip). Among these dislocation loops, the expansions of only types 1 and 5 contribute to easy-glide slip. Consideration of crystal geometry [15] suggests that the CRSS for type 5 slip is substantially greater than it is for type 1 slip. Briefly, if plastic deformation were to occur by simple shear during type 5 slip, rows of iodine atoms in neighbouring monoatomic planes would slip directly over one another, at a nearest interatomic approach of 0.272 nm. Simple shear by type 1 slip would cause the rows of iodine atoms on one side of the slip plane to pass over the "valleys" between iodine rows on the other side; the nearest interatomic approach would be 0.348 nm. In a perfect crystal the iodine atoms in adjacent layers are 0.411 nm apart. Since iodine–iodine repulsion should increase as the interatomic distance is reduced, type 5 slip should require considerably more stress than type 1 slip. Furthermore, measurements [15] of the directional dependence of stresses required to cause slip on (0 0 1) planes of thin single crystals of HgI_2 were consistent with the usual Schmid law, wherein slip occurs by the movement of (0 0 1)$a\langle 1\,0\,0\rangle$ dislocations (i.e. type 1 slip) for shear loading in any direction parallel to the (0 0 1) plane. Thus the CRSS for type 5 slip is expected to be at least a factor of $2^{1/2}$ more than for type 1 slip.

With regard to the hard-glide slip systems, an examination of the crystal structure suggests that slip over {1 0 0} planes should be easier than slip over {1 1 0} planes. The interplanar covalent bond density of {1 1 0} planes is $2\,(2^{1/2})/ac$ while that of {1 0 0} planes is $2/ac$, where ac is the area of a large unit-cell face. Neighbouring {1 1 0} planes are monoatomic and alternate in species; each Hg atom must simultaneously deform two of its four covalent bonds for {1 1 0} slip to

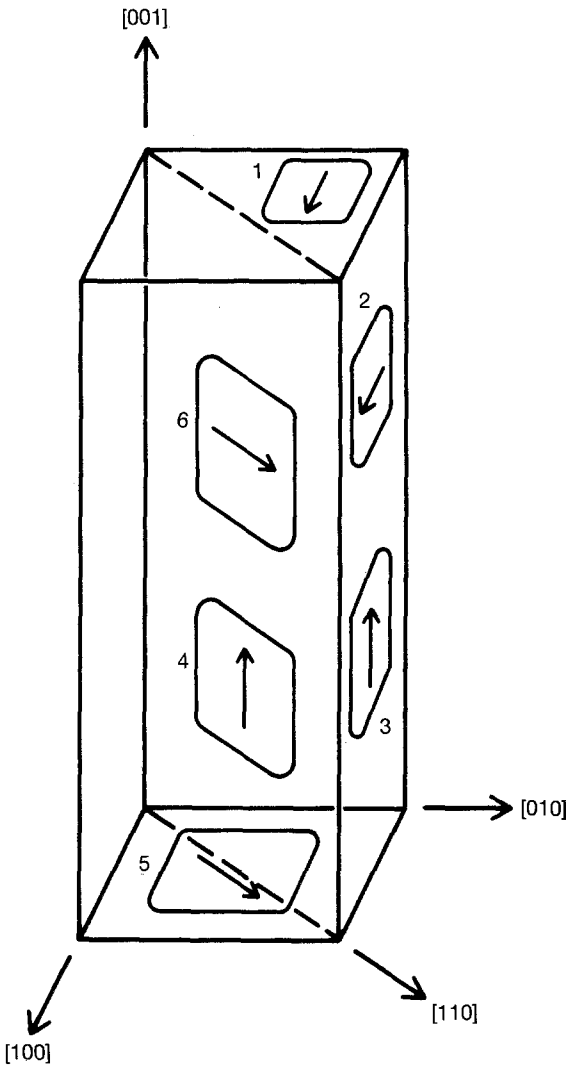

Figure 8 Illustration showing the dislocation loops and Burgers vectors of six types of potential slip system in single-crystal HgI_2 (from Georgeson and Milstein [13]).

TABLE III Compilation of slip systems considered in the present study, listed in presumed order of increasing critical resolved shear stress[a]

Slip type	Slip systems: (plane) [direction]	
1 (easy glide)	(0 0 1) [1 0 0]	(0 0 1) [0 1 0]
5 (easy glide)	(0 0 1) [1 1 0]	(0 0 1) [1 $\bar{1}$ 0]
2 (hard glide)	(0 1 0) [1 0 0]	(1 0 0) [0 1 0]
3 (hard glide)	(0 1 0) [0 0 1]	(1 0 0) [0 0 1]
6 (hard glide)	(1 $\bar{1}$ 0) [1 1 0]	(1 1 0) [1 $\bar{1}$ 0]
4 (hard glide)	(1 $\bar{1}$ 0) [0 0 1]	(1 1 0) [0 0 1]

[a] For each type of slip there are two specific slip systems, corresponding to the two geometrically similar (and perpendicular) slip directions (for the easy-glide types of slip) or slip planes (for the hard-glide types). The first system listed in each case corresponds to that illustrated in Fig. 8. Slip systems such as (0 0 1) [1 0 0] and (0 0 1) [$\bar{1}$ 0 0], which have the same slip planes but opposite slip directions, are considered to be the same specific system.

occur. During {1 0 0} slip, each Hg atom must break and reform only one of its four covalent bonds. The spacing between neighbouring {1 1 0} planes is smaller than between {1 0 0} planes ($a/[2(2^{1/2})]$ versus $a/2$) and so from the viewpoint of a hard sphere model, {1 1 0} planes are more interlocked with one another than are {1 0 0} planes.

For slip of either the {1 0 0} or the {1 1 0} planes arguments can be made, on the basis of the number and proximity of interatomic encounters per unit slip area, that slip in the [0 0 1] direction requires the most stress. Consider, for the moment, solely the strong, covalent near-neighbour interactions between Hg and I atoms. In their equilibrium configuration, near-neighbour Hg and I atoms are 0.278 nm apart. Type 3 slip over an area *ac* requires four distinct separations and close encounters, at an ideal maximum separation of 0.378 nm and nearest approach of 0.218 nm. In contrast, type 2 slip necessitates the breaking and reforming of only two covalent bonds over the same slip area [13], at a minimum approach of 0.278 nm (i.e. equilibrium spacing) and a maximum separation of 0.353 nm. In a similar fashion, for {1 1 0} planes, type 4 slip should be more difficult than type 6 slip, since type 4 slip over an area $ac\ 2^{1/2}$ requires eight individual separations and close encounters between unlike atoms (maximum separation of 0.378 nm and nearest approach of 0.218 nm), while type 6 slip requires only four of each (at a maximum separation of 0.385 nm and a minimum approach of 0.232 nm). The conclusions stated in the above paragraphs are readily verified with the aid of the crystal structure illustrations found elsewhere [13, 15].

These arguments lead to an expected ordering of the CRSS magnitudes in the following sequence: type 1 < type 5 ≪ type 2 < type 3 < type 6 < type 4. When a hardness indentation is made at a particular orientation on a given crystallographic plane, plastic deformation by slip occurs on those slip systems for which the shear stress applied by the indentor exceeds the critical value required to cause slip. The size of the indentation, and hence the measured hardness of the crystal, depends on the volume of material that has slipped, which in turn depends on the volume of the crystal over which the shear stress is sufficient to cause slip. The actual stress and displacement fields in the vicinity of a Knoop indentation are complex. However, insight into the anisotropy of Knoop microhardness can be gained by determining an approximate stress field for the indentor and then using this stress field to compute the spatial dependence of the resolved shear stresses acting upon relevant slip systems, as a function of indentor orientation. In order to determine the stress fields, we follow Roberts *et al.* [12] who approximated the stress field of a Knoop indentor by that of an infinite flat punch in elastic contact with the flat surface of an elastically isotropic medium (the IFP model). As discussed by them [12], this model is a considerable simplification of the real situation; single crystals are generally elastically anisotropic, Knoop indentors have an elongated pyramidal shape and finite dimensions, and real stress fields include contributions from the plastic zone which forms around the indentor during loading. Nevertheless, when combined with information about relevant slip systems, the model has been able to explain satisfactorily most of the observed trends in Knoop microhardness anisotropy, for a variety of crystalline materials [12, 16–18].

The coordinate system associated with the IFP is shown in Fig. 9. A uniform load P is applied to the punch, which is of infinite length (in the $\pm z$ direction) and of width $2w$ (reckoned coincident with the x axis); the punch is brought into contact with the xz (or $y = 0$) surface of the material. The Cartesian stress components σ_{ij}, at a point $R(x, y)$ in the material, are given by [19]

$$\sigma_{xx} = -\frac{P}{2\pi}[2(\Phi_1 - \Phi_2) + \sin 2\Phi_1 - \sin 2\Phi_2]$$

$$\sigma_{yy} = -\frac{P}{2\pi}[2(\Phi_1 - \Phi_2) - \sin 2\Phi_1 + \sin 2\Phi_2]$$

$$\sigma_{xy} = \sigma_{yx} = \frac{P}{2\pi}(\cos 2\Phi_1 - \cos 2\Phi_2)$$

$$\sigma_{zz} = \nu(\sigma_{xy} + \sigma_{yx})$$

where ν is Poisson's ratio for the loaded material and the angles Φ_1 and Φ_2 are as defined in Fig. 9. In order to use the IFP model to compute the relative stress magnitudes on the different, potentially active, slip systems, the numerical values of P, ν and w were assigned arbitrarily as 100, 1/3 and 2, respectively; all stress values calculated with the IFP model thus have the same (arbitrary) dimensional units as P.

Two sets of computations were made: one for the case where the plane upon which the punch acts (i.e. the $y = 0$ plane) was taken as the (0 0 1) crystal face and the other for this plane taken to be the (1 1 0) crystal face. For each set, computations were made over a range of punch orientations. The infinite z axis of the punch is defined to be coincident with the long diagonal of the Knoop indentor. With this identity, the z axes and orientation angles θ, shown in Fig. 1a and b for the Knoop indentor, also apply for the IFP. These geometric parameters are shown in Fig. 10 for the IFP, relative to the crystal axes $[h\,k\,l]$ and to the

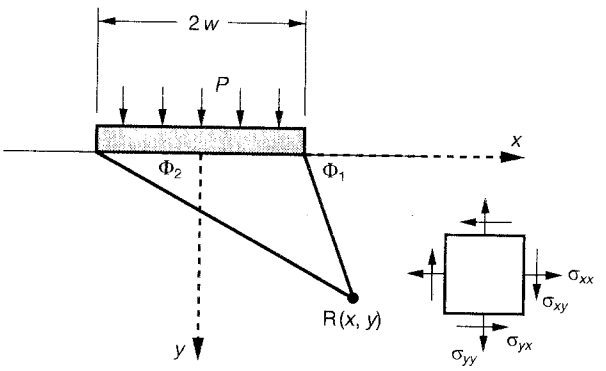

Figure 9 Coordinate system used to compute the stress components in the infinite flat punch (IFP) model. (Stress component σ_{zz}, which is perpendicular to the plane of this figure, is not shown.) The $y = 0$ plane is coincident with the surface of the crystal.

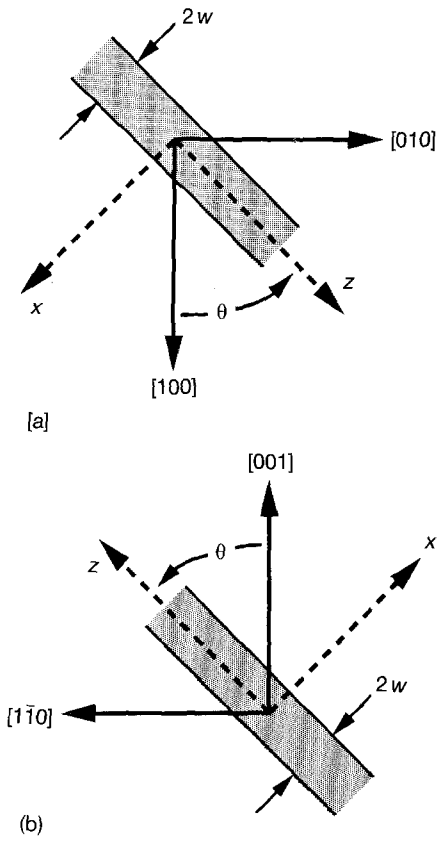

Figure 10 Planar views of the punch orientation for indentions on (a) the (0 0 1) surface and (b) the (1 1 0) surface of the crystal. In each case the surface of the crystal (i.e. the xz plane) is coincident with the plane of the figure.

Cartesian axes employed in the computation of the σ_{ij} values. For each punch orientation, values of σ_{xx}, σ_{yy}, σ_{xy} and σ_{zz} were computed at 3660 positions $R(x, y)$, in a span of material beneath the punch ranging from $x = 0$ to $3w$ and $y = 0$ to $3w$. These values were, in turn, used to compute the resolved shear stresses on the relevant slip systems tabulated in Table III, at each of these 3660 points in the material. These resolved shear stresses are designated as $\sigma_{(hkl)[h'k'l']}$ to indicate a shear stress σ acting on the plane (hkl) in the direction $[h'k'l']$.

For the particular slip systems listed in Table III, static equilibrium requires that $\sigma_{(hkl)[h'k'l']} = \sigma_{(h'k'l')[hkl]}$. Thus, owing to these symmetries, every set of resolved shear stress computations for a particular easy-glide slip system is also applicable to a specific hard-glide system; thus, for example, the resolved shear stress at a given point in the material on the (0 0 1) [1 0 0] type 1 slip system is the same as that on the (1 0 0) [0 0 1] type 3 slip system. While easy-glide slip undoubtedly occurs during the penetration of a Knoop indentor into the surface of HgI_2, some slip over hard-glide systems must also take place. The relative importance of easy-glide *vis-à-vis* hard-glide slip is discussed below in Section 4. Here we mention briefly that, owing to the much greater resolved shear stress required for hard-glide slip, it is the response of the hard-glide slip systems that apparently will control the size of the Knoop indentation. In our presentation of the resolved shear stresses that apply to both an easy and a hard-glide system, both systems are specified (for completeness), but it is the stress response on the hard-glide system that is of particular concern.

The resolved shear stresses, computed with the IFP model as described above, were used to make (i) contour maps in an xy plane (i.e. a plane normal to the infinite axis of the punch) of the shear stresses on the slip systems, at particular angles θ; (ii) plots showing the variation of shear stress on the slip systems, as a function of θ, at particular locations $R(x, y)$ beneath the punch; and (iii) plots of the relative volume of material Ω containing potentially active slip systems subjected to shear stresses greater than a specific CRSS value, versus punch orientation θ. These calculated behaviours were examined, for each slip system, to determine whether the resolved shear stress on the slip system varies with θ in a manner that is consistent or inconsistent with the experimental Knoop microhardness data. We assume that consistency occurs when the shear stress magnitudes, over relatively large regions of the crystal, vary with θ in an inverse relation to the measured microhardness (i.e. increasing stress magnitudes coinciding with decreasing microhardness values).

3.1. IFP calculations for the (0 0 1) surface

Examples of plots of the calculated resolved shear stresses (on the slip systems of Table III) versus orientation angle θ, for the punch in contact with the (0 0 1) surface, are shown in Figs 11 and 12. These curves are calculated for a particular point $R(x, y) = R(w, w)$ reckoned relative to the punch coordinates, and are thus intended mainly to show the essential symmetries, including the locations of stress magnitude maxima and zeros.

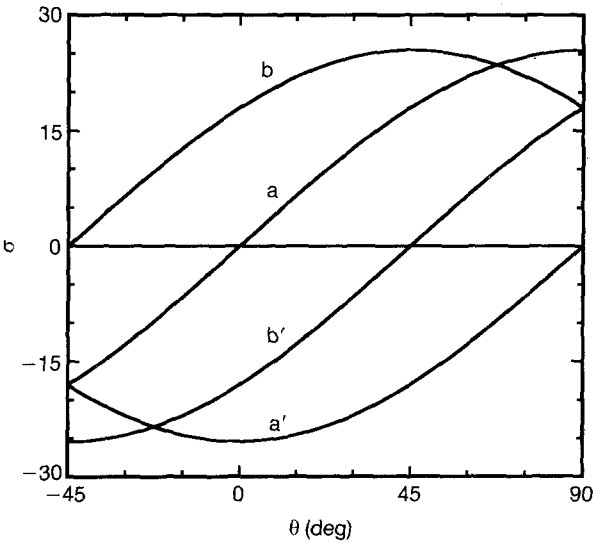

Figure 11 Resolved shear stresses on slip systems of types 1, 3, 4, and 5 versus orientation angle θ, for a punch acting on the (0 0 1) face of HgI_2, for the particular coordinate $R(x, y) = R(w, w)$ in the material. The slip systems are as follows: (a) (1 0 0)[0 0 1] (type 3) and (0 0 1)[1 0 0] (type 1), (a′) (0 1 0)[0 0 1] (type 3) and (0 0 1)[0 1 0] (type 1), (b) (1 $\bar{1}$ 0)[0 0 1] (type 4) and (0 0 1)[1 1 0] (type 5), and (b′) (1 1 0)[0 0 1] (type 4) and (0 0 1)[1 1 0] (type 5).

In Fig. 11, curves a and a′ each describe the resolved shear stress acting on a type 3 and a type 1 slip system; curve a shows the shear stress on the (1 0 0) [0 0 1] type 3 and the (0 0 1) [1 0 0] type 1 slip systems while curve a′ shows the shear stress on the (0 1 0) [0 0 1] type 3 and the (0 0 1) [0 1 0] type 1 slip systems. Since the slip planes of the two type 3 systems are perpendicular (as are the slip directions of the two type 1 systems), curves a and a′ are 90° "out of phase." For purposes of discussion, the curves a and a′ (and their associated slip systems) are referred to as "complementary." Curve b, which describes the resolved shear stresses on the (1 $\bar{1}$ 0) [0 0 1] type 4 and (0 0 1) [1 $\bar{1}$ 0] type 5 slip systems, is similarly complementary to curve b′, which applies to the (1 1 0) [0 0 1] type 4 and (0 0 1) [1 1 0] type 5 slip systems. In Fig. 11, the slip systems described by curve a′ (the "a′-slip systems") are subjected to their greatest shear stress magnitudes when $\theta = 0°$, while the complementary a-slip systems are unstressed. In the range of $-45° < \theta < 45°$, the shear stress magnitudes on the a′-slip systems are greater than those on the a-slip systems, and thus for these orientations, the a′-slip systems are more likely than the a-slip systems to undergo slip. If $\theta = \pm 45°$, the shear stress magnitudes on the a- and the a′-slip systems are equal; then slip on either system is equally likely. Also, as θ departs from 0° in either direction, the stress magnitude on the a′-slip systems decreases. Note that this behaviour is consonant with the experimentally observed variation of H_K with θ in Fig. 2; i.e. as θ varies from 0 to $\pm 45°$, a decreasing shear stress magnitude on curve a′ in Fig. 11 can be associated with an increasing microhardness (a smaller indentor penetration) in Fig. 2. (Although the shear stress magnitudes on the type 3 and 1 a-slip systems increase as θ departs from 0°, this behaviour would be expected to have only a secondary effect upon the orientational dependence of the Knoop microhardness in the range $-45° < \theta < 45°$, since as indicated above, the effect of the (larger) stresses on the type 3 and 1 a′-slip systems would be expected to dominate any behaviour that results from any type 3 or 1 slip.)

In contrast to the behaviour of the type 3 and 1 a′-slip systems, if slip on b- and/or b′-slip systems were to control the degree of penetration, curves b and b′ in Fig. 11 would imply that H_K should increase as θ varies from 0 to $\pm 45°$, which was not observed experimentally. In particular, at $\theta = 0°$, both the b- and b′-slip systems are subjected to the same stress magnitudes. In the range $0° < \theta < 90°$, the b-slip systems are more likely to yield than the b′-slip systems, and vice versa in the range $-90° < \theta < 0°$. However, as θ increases from 0° (in the range 0 to 45°), the resolved shear stress on the b-slip systems increases, which would be expected to cause increased yielding of the crystal if this type of slip were predominant, and similarly for the b′-slip systems in the range 0 to $-45°$.

Fig. 12 shows the resolved shear stresses on the slip systems of type 2 and 6, as a function of punch orientation, at the point $R(x, y) = R(w, w)$. Comparisons of Figs 2 and 12 show that slip by the systems described by curve c (type 6) is consonant with the experimental data while that of curve d (type 2) is not. That is, at

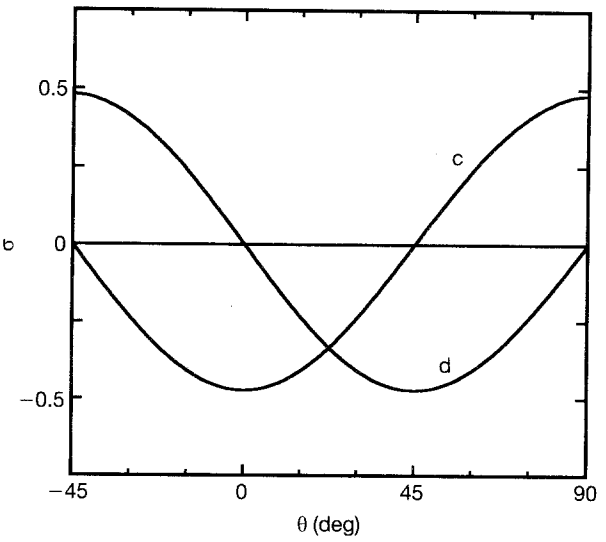

Figure 12 Resolved shear stresses on slip systems of types 2 and 6 versus orientation angle θ, for a punch acting on the (0 0 1) face of HgI_2, for the particular coordinate $R(x, y) = R(w, w)$ in the material. The slip systems are as follows: (c) (1 1 0)[1 $\bar{1}$ 0] and (1 $\bar{1}$ 0)[1 1 0] (type 6) and (d) (1 0 0)[0 1 0] and (0 1 0)[1 0 0] (type 2).

$\theta = 0°$ the magnitude of curve c is at a maximum whereas that of curve d is zero. However, it is also observed that the shear stress amplitudes of both curves c and d are more than an order of magnitude lower than those of curves a and a′ in Fig. 11.

Among the hard-glide slip systems represented in Figs 11 and 12, only types 3 and 6 have shear stress variations that are consistent with the experimental data. However, the critical shear stress required for type 6 slip is expected to exceed that for type 3 slip (as discussed earlier, based upon crystal symmetry and bonding considerations), whereas the shear stresses calculated for type 6 slip systems (curve c in Fig. 12) tend to be much less than those for type 3 (curves a and a′ in Fig. 11). These results imply that type 3 slip systems are more likely to participate in the plastic deformation at a Knoop impression than are the type 6 slip systems. This conclusion is also supported by the numerous contour plots that were made of the spatial dependence of resolved shear stress acting on the relevant slip systems. A few examples of such contour plots are shown in Figs 13 and 14. Fig. 13a and b show the magnitudes of the shear stress on the type 3 slip system associated with curve a′ at $\theta = 0$ and 45°, respectively. It is clear from these plots that the magnitudes of the resolved shear stress applied to this slip system are greater, over a larger region of material, when the punch is at $\theta = 0°$. Fig. 14 shows the shear stress contours for type 6 slip at $\theta = 0°$ (the orientation where the resolved shear stress on type 6 slip systems is largest). Comparison of this figure with Fig. 13a and b shows that the bulk of the material in the vicinity of the punch is subjected to considerably lower stress magnitudes on the type 6 slip systems than on the relevant type 3 system.

Finally, plots were made of the relative volume Ω of the activated type 3 slip systems as a function of orientation angle θ. The relative volume Ω of activated

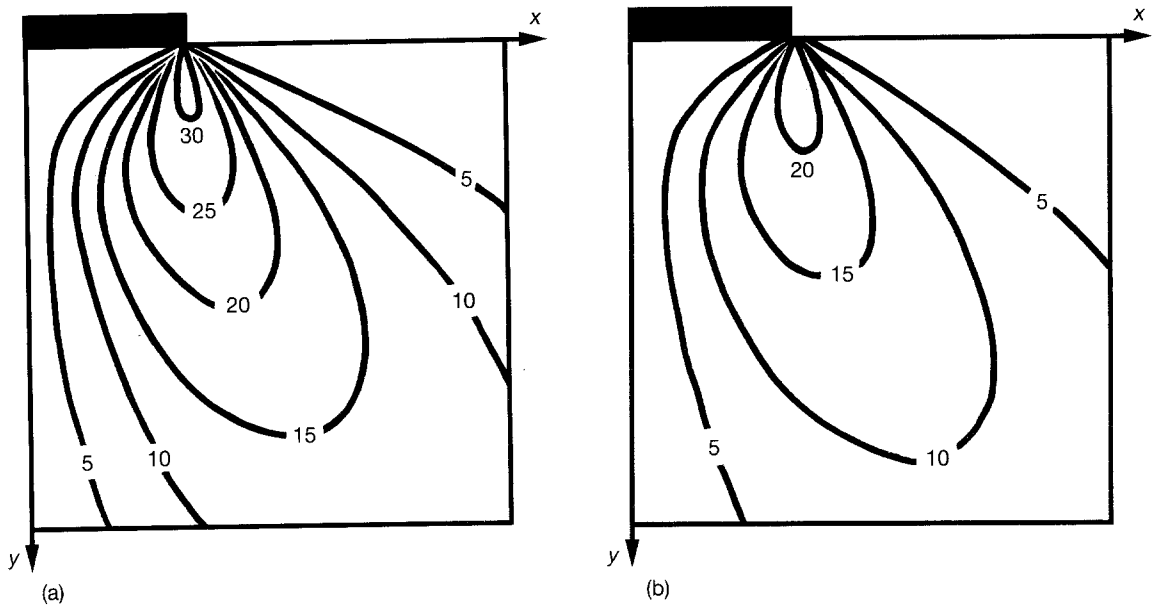

Figure 13 Contour plots of constant resolved shear stress magnitude, on the type 3 slip system associated with curve a′ in Fig. 11, calculated for the IFP acting on the (0 0 1) plane of HgI_2: (a) $\theta = 0°$; (b) $\theta = 45°$. (These are also the resolved shear stress magnitudes on (1 1 0)[0 0 1] type 4 and (0 0 1)[1 1 0] type 5 slip systems for the IFP acting on the (1 1 0) plane at (a) $\theta = 90°$ and (b) $\theta = 45°$, as discussed in section 3.2.)

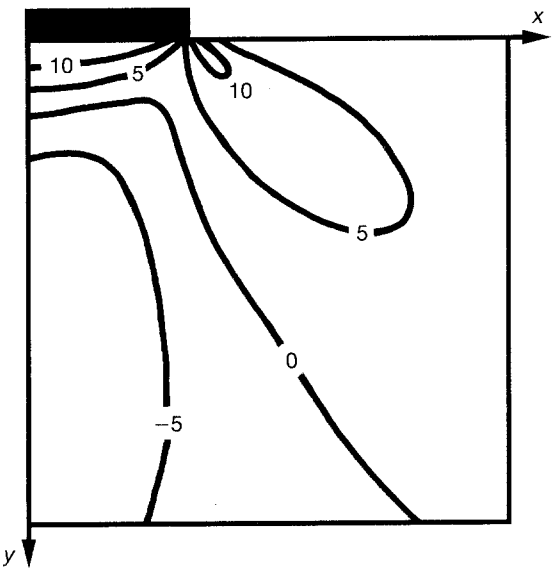

Figure 14 Contour plots of constant resolved shear stress on slip systems of type 6, calculated for the IFP acting on the (0 0 1) plane of HgI_2 at $\theta = 0°$.

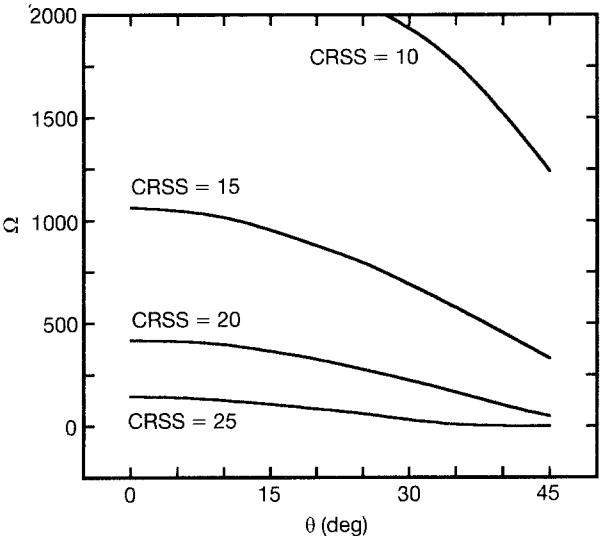

Figure 15 Orientation dependence of the relative volume Ω of activated type 3 slip systems for the IFP applied to the (0 0 1) plane of HgI_2.

slip for a particular type of slip system is defined as that set of points on the contour plots for which the resolved shear stresses exceed a specified CRSS value on one (or both) of the specific slip systems of the type under consideration. An area of w^2 (with $w = 2$) on the contour plots corresponds to $\Omega = 400$ (i.e. it contains 400 points of computation $R(x, y)$). Plots of Ω versus θ for type 3 slip are shown in Fig. 15 for CRSS values of 10, 15, 20 and 25. (For example, at a punch orientation of 30°, say, the relative volume of activated type 3 slip is 1938, 690, 224 and 31 when the CRSS required for activation of type 3 slip is taken as 10, 15, 20 and 25, respectively.) According to our initial hypothesis, the theoretical variation of Ω with θ should be inverse to the experimental variation of H_K with θ. Comparison of Figs 2 and 15 corroborates this hypothesis nicely.

3.2. IFP calculations for the (1 1 0) surface

The interpretation of the orientation dependence of microhardness for indentions on the (1 1 0) surface, in terms of IFP model calculations, is more complex than that for indentions on the (0 0 1) surface, owing to lesser symmetry in the former case. For the IFP applied to the (1 1 0) surface, the slip systems that were found to be inconsistent with the experimental results (i.e. on which the resolved shear stress magnitudes did

not vary inversely with the measured microhardness values) are the types 2 and 6, the specific type 4 given by $(1\,\bar{1}\,0)$ [0 0 1] and the specific type 5 given by (0 0 1) [1 $\bar{1}$ 0]. Both types 2 and 6 slip systems exhibit maximum shear stress magnitudes at $\theta = 0°$; the specific slip systems of types 4 and 5 mentioned above are unstressed at both $\theta = 0°$ and $\theta = 90°$, and are under their greatest stress at $\theta = 45°$. Thus each of these slip systems, taken individually, acts in a manner contradictory to observation.

Calculated IFP shear stress variations on the remaining slip systems are shown in the contour plots of Figs 13 and 16–18. The shear stresses on the (1 1 0) [0 0 1] type 4 (and the (0 0 1) [1 1 0] type 5) slip systems are shown in Fig. 13a and b for $\theta = 90$ and 45°, respectively; no shear stresses act on these systems at $\theta = 0°$. Figs 16a and b, 17a and b and 18 show the shear stress distributions on the type 3 (and type 1) slip systems at $\theta = 30$, 60 and 90° (these systems are unstressed at $\theta = 0°$). For all of these slip systems, as θ increases from 0°, greater volumes of material tend to be subjected to greater shear stress magnitudes. Thus, the shear stress variations on the type 3 and the specific (1 1 0) [0 0 1] type 4 hard-glide slip systems can be considered to be generally consistent with the observed variations of H_K, although some important distinctions can be made. First, among the hard-glide systems, the CRSS required for slip is presumably very much greater for the type 4 than for the type 3 systems, as is discussed in the first part of this section. This consideration, in itself, makes it unlikely that type 4 slip dominates the indention process. Second, the

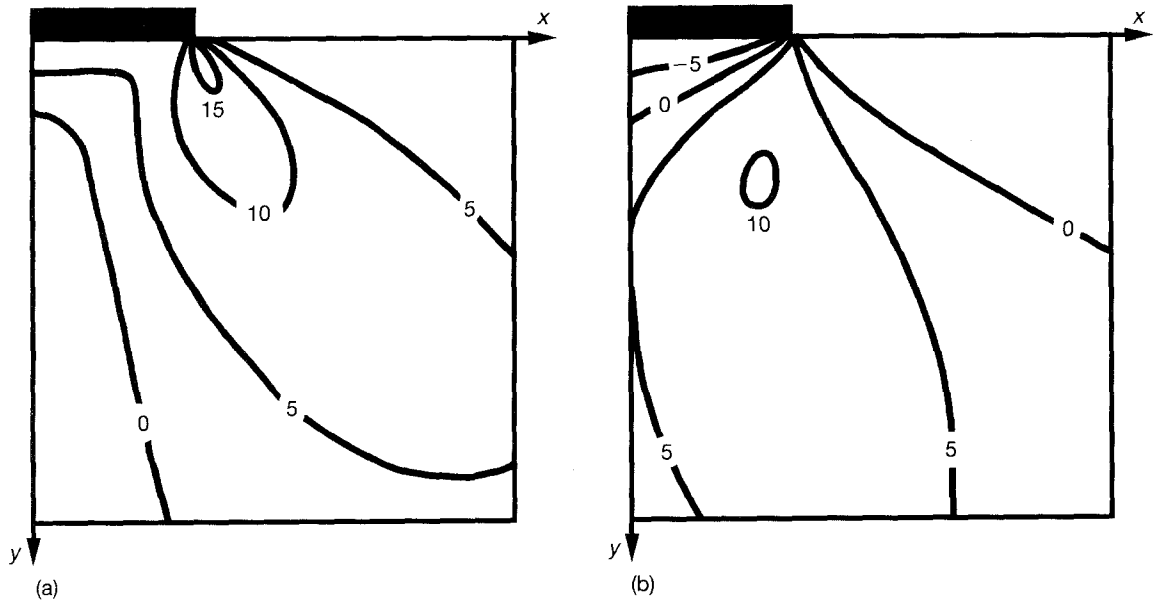

Figure 16 Contour plots of constant resolved shear stress on the (a) type 3 (1 0 0)[0 0 1] (or type 1 (0 0 1)[1 0 0]) and the (b) type 3 (0 1 0)[0 0 1] (or type 1 (0 0 1)[0 1 0]) slip systems, calculated for the IFP acting on the (1 1 0) plane of HgI_2, at $\theta = 30°$.

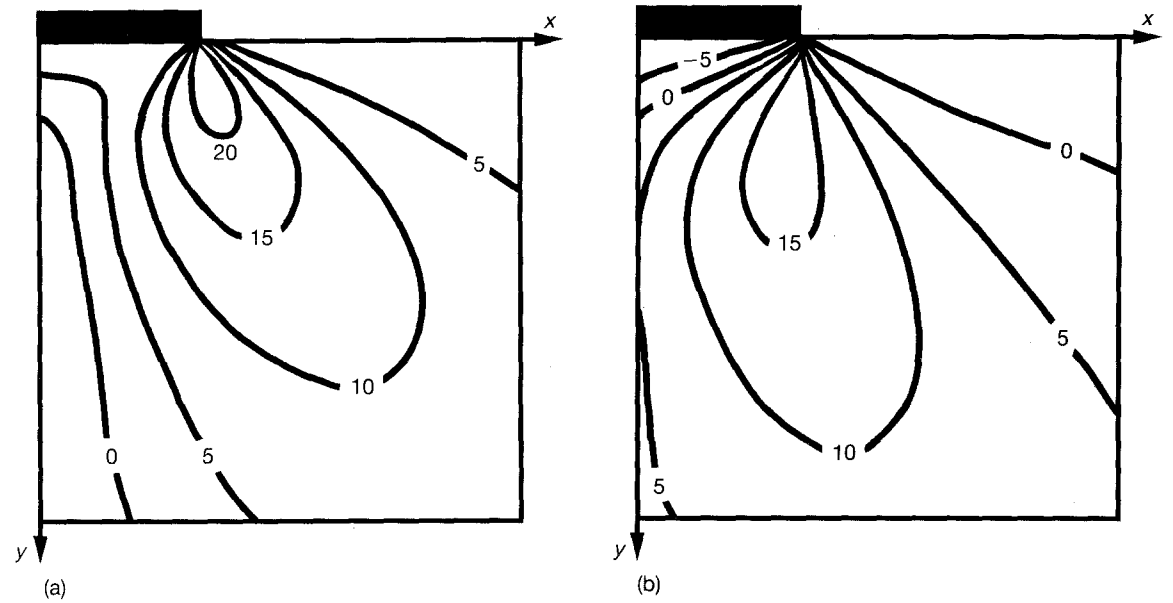

Figure 17 Same as Fig. 16 but for $\theta = 60°$.

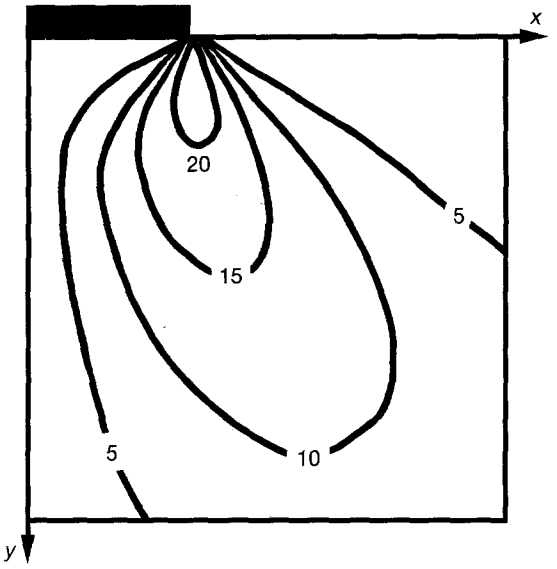

Figure 18 Same as Fig. 16 but for $\theta = 90°$; the resolved shear stress distribution is the same on all type 1 and type 3 slip systems.

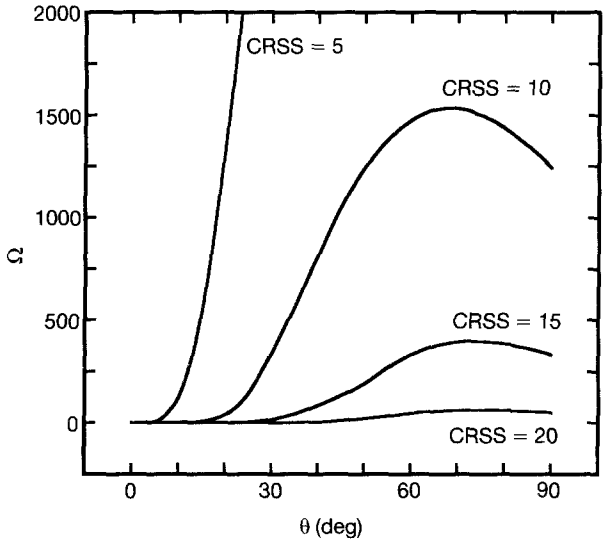

Figure 19 Orientation dependence of the relative volume Ω of activated type 3 slip systems for the IFP acting on the (1 1 0) plane of HgI_2.

θ dependence of the shear stress distributions on the (1 1 0) [0 0 1] type 4 (and (0 0 1) [1 1 0] type 5) slip systems predicts a hardness minimum at $\theta = 90°$. Although this can be considered as consistent with the experimental data, correlation with a hardness minimum at $\theta \simeq 75°$, which the average microhardness values exhibit (Fig. 4), cannot be found in these stress distributions. However, based upon the criterion that the size of an indention depends upon the localized volume of material over which the resolved shear stress exceeds the CRSS for the relevant slip systems, a hardness minimum does occur in the IFP computations for the type 3 (and 1) slip systems. This is explained below.

Fig. 19 shows the relative volume Ω of type 3 activated slip, as a function of punch orientation θ, for the punch applied to the (1 1 0) plane. This figure was constructed in a manner similar to Fig. 15. Thus, for example, at a punch orientation of $\theta = 60°$ the relative volumes of material in which (at least) one type 3 slip system is subjected to resolved shear stresses greater than 5, 10, 15 and 20 are, respectively, 3208, 1490, 336 and 47. The curves in Fig. 19 have two interesting features. First, they exhibit a maximum that moves to larger values of θ as the presumed CRSS of the slip systems increases and second, the curves have the same general shape as the inverse of the H_K versus θ curve shown in Fig. 4. That is, as θ increases from 0°, both H_K and Ω initially vary slowly; thereafter, both exhibit relatively rapid variations, over a span of about 30°, on their approach to an extremum; in the vicinity of this extremum, both again vary slowly. Since the IFP model is only a crude approximation to the Knoop indentor, one should not read too much into such details as the specific locations of the maxima in Fig. 19. Nevertheless, the strong resemblance between the curves of Figs 4 and 19 is striking.

4. Discussion and conclusions

The formation of a Knoop impression on a crystalline surface requires, in general, plastic deformation over multiple independent slip systems. The extent to which each possible slip system contributes to the formation of a Knoop indentation is, no doubt, a complicated function of many factors including the CRSS value of each system, the stress distribution on each system, and the interactions of various slip systems with each other and with crystal imperfections (i.e. work-hardening). It is not the intention here to make a detailed analysis of all possible contributions to the plastic deformation induced by a Knoop indentor on an HgI_2 surface. Rather, we concentrate on the salient results derived from the IFP model and their correlation with the experimental data.

The results of the IFP calculations, presented in the previous section, demonstrate that an inverse relationship exists between (i) the intensity of the shear stresses acting on type 3 and type 1 slip systems at particular punch orientations, and (ii) experimental Knoop microhardness measurements made at corresponding indentor orientation angles, on both the (0 0 1) and (1 1 0) planes of HgI_2. That is, when the relative volume of material that is stressed past a presumed CRSS on these types of slip system is large, the measured values of H_K are low (the indentions are large) and when this relative volume is small, H_K is high (small indentions). Type 3 and type 1 slip systems are the only slip systems for which IFP model calculations reveal this inverse relationship with Knoop microhardness for both the (0 0 1) and (1 1 0) planes of HgI_2.

Because the relation $\sigma_{(hkl)[h'k'l']} = \sigma_{(h'k'l')[hkl]}$ holds for the slip systems considered in this study, the stress distributions calculated for the type 1 systems given by (0 0 1) [1 0 0] and (0 0 1) [0 1 0] will always be identical, respectively, to those for the type 3 systems (1 0 0) [0 0 1] and (0 1 0) [0 0 1]. However, for a given stress distribution, the resistance to shear over type 3 systems will be much higher than over type 1 systems, since the former is a hard-glide slip system while

the latter is an easy-glide slip system. If the microhardness H_K is taken as a rough estimate of the level of stress generated by a penetrating Knoop indentor ($\sim$100 to 300 MPa) and if the CRSS for type 1 slip is estimated from the typical yield points observed during shear testing of single crystals of HgI_2 over (0 0 1) planes ($\sim$0.1 to 0.5 MPa [2, 5, 15]), then it is reasonable to conclude that the CRSS of type 1 slip systems is routinely exceeded within the material near a Knoop indentation. The experimentally observed slip lines (aligned with $[1\bar{1}0]$), induced during microhardness measurements on (1 1 0) crystal faces, support this view by demonstrating that the CRSS for easy-glide slip is exceeded over an extended region around each indention, regardless of indentor orientation. The primary resistance to indentor penetration of the HgI_2 surface is thus provided by hard-glide rather than the easy-glide slip systems; i.e. the extent of hard-glide slip determines the size of an indentation. The observed orientation dependence of Knoop microhardness is therefore attributed to the orientational variation of the resolved shear stress distributions on the type 3, rather than type 1, systems. This is not to say that type 1 slip is unimportant in the formation of a Knoop impression; the slip systems of type 3 and type 1 are independent. For Knoop indentions on (0 0 1) faces, type 1 slip moves material parallel to the surface while type 3 slip punches material into the bulk (by slip over {1 0 0} planes); for indentions on {1 1 0} planes, type 3 slip displaces material parallel to the surface (over {100} planes) while type 1 slip proceeds, over (0 0 1) planes, into the material. In summary we conclude that, while easy-glide slip no doubt occurs during the indention process, it is the hard-glide slip of type 3 that limits the ultimate size of a Knoop indentation (and so determines the microhardness).

With this conclusion we can sharpen our understanding of details in the experimental results. For the hazy crystals, on (0 0 1) planes H_K varies from 11.1 to 13.2 as θ goes from 0 to 45°, whereas the variation of H_K is much stronger on {1 1 0} planes, ranging from 28.6 at $\theta = 0°$ to 13.5 at $\theta = 90°$, with a minimum value of about 12.7 at $\theta = 75°$. Theoretically, during loading of the (0 0 1) surface by an IFP, at least one of the two type 3 slip systems will always be stressed, regardless of punch orientation. This condition is reflected in the θ-dependence of the relative volume Ω, which is loaded past a presumed CRSS value on type 3 slip systems, as seen in Fig. 15. For example, for a CRSS of 15, say, Ω decreases monotonically from 1064 at $\theta = 0°$ to 330 at $\theta = 45°$; at any punch orientation a significant volume of the material beneath the indentor is stressed past the CRSS. This contrasts with the IFP loading the (1 1 0) plane, wherein both specific type 3 systems are simultaneously unstressed at the orientation angle $\theta = 0°$. The IFP calculations for the (1 1 0) surface, based upon a CRSS of 15, give $\Omega = 0$ at $\theta = 0°$ and $\Omega = 330$ at $\theta = 90°$, with a maximum value of $\Omega \simeq 400$ at about 72°, as Fig. 19 shows. Thus, for {1 1 0} planes, the high value of $H_K = 28.6$ at $\theta = 0°$ correlates well with the zero resolved shear stress computed for type 3 slip systems in this orientation.* The lower values and the more gradual angular variation of H_K on (0 0 1) planes occur because the resolved shear stress for type 3 slip is never zero. Furthermore, when $\theta = 45°$ on the (0 0 1) plane and when $\theta = 90°$ on the (1 1 0) plane, the relative volumes Ω of the type 3 slip systems stressed past any given CRSS value are the same for both planes. We thus conclude, theoretically, that the experimental values of H_K should be approximately equal for the corresponding indentor orientations. This agreement indeed occurs (i.e. $H_K = 13.2$ on the (0 0 1) plane at $\theta = 45°$ and $H_K = 13.5$ on the (1 1 0) plane at $\theta = 90°$). Although no attempt was made to determine an optimum CRSS value, for comparison with the experimental results, CRSS values in the range of about 10 to 25 are seen to scale reasonably well with the experimental data. When the CRSS is taken to be 15, say, the theoretical and experimental behaviours agree quite well in the neighbourhood of the H_K minimum (Ω maximum) for indentions on the (1 1 0) planes. For example, on this plane the values of H_K are approximately equal at $\theta = 60$ and 90°, as are the theoretical values of Ω at these orientations (when the CRSS = 15).

In summary, for indentions on both the (0 0 1) and the (1 1 0) planes of HgI_2, the calculations of the IFP model, as well as considerations of behaviour expected from known crystal symmetry and interatomic bonding, give a comprehensive understanding of the experimentally determined variation of H_K with indentor orientation, based on penetration controlled mainly through the movement of material via type 3 slip systems.

Appendix: Theory of the orientation dependence of H_K on the (1 0 0) and (1 0 1) planes of HgI_2

In view of the excellent correlation between theory and experiment for Knoop microhardness indentions on the (0 0 1) and (1 1 0) planes of HgI_2, it is considered worthwhile to extend the theoretical computations for type 3 slip to indentions on other crystallographic planes. This was done for the (1 0 0) and (1 0 1) planes, as part of the present study; the results are as follows. For the IFP loading the (1 0 0) plane, both type 3 slip systems are unstressed when the punch is aligned with the [0 0 1] direction ($\theta = 0°$) and the specific type 3 system given by (1 0 0) [0 0 1] is under the maximum stress when the punch is aligned with $[0\bar{1}0]$ ($\theta = 90°$). The relative volume Ω stressed past a given CRSS is zero at $\theta = 0°$ and reaches a maximum value when θ is increased to 90°. Thus, the experimental values of H_K are expected to be highest at $\theta = 0°$ and lowest at

* Possible reasons why H_K does not become arbitrarily large as θ goes to zero on the (1 1 0) surface are, first, that slip systems other than the type 3 systems may play some role in the Knoop indention process as θ approaches zero; and second (and perhaps most important), even though the simple geometry of the IFP predicts zero shear stress for the punch in contact with the (1 1 0) plane at $\theta = 0°$, during an actual Knoop microhardness test the elongated pyramidal shape of the indentor will no doubt cause some activation of type 3 slip.

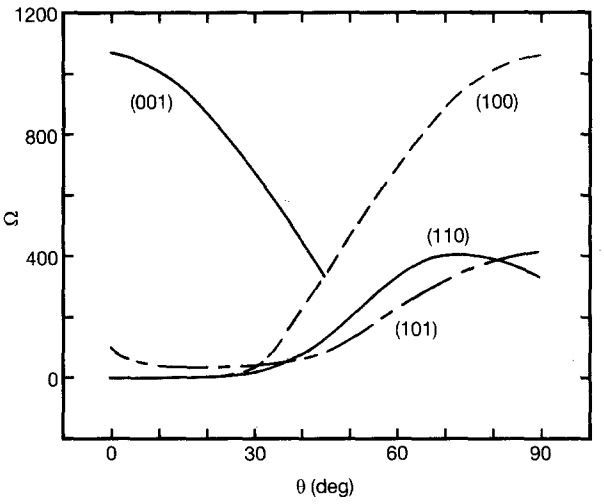

Figure A1 Orientation dependence of the relative volume Ω of activated type 3 slip, when the CRSS is 15, for the IFP acting on various crystal surfaces (*h k l*).

$\theta = 90°$, with no intermediate extremum. For a CRSS of 15, IFP model calculations give $\Omega = 330$ at $\theta = 45°$ and $\Omega = 1064$ at $\theta = 90°$, as seen in Fig. A1. (The function $\Omega(\theta)$ for the (0 0 1) plane in the range $\theta = 0$ to 45° is, in fact, symmetric with the function $\Omega(\theta)$ for the (1 0 0) plane in the range $\theta = 45$ to 90°.) Since H_K varies in an inverse manner with Ω, H_K on the (1 0 0) plane is expected to drop substantially as θ varies from 0 to 45° and to decrease more gradually over the range 45 to 90°. For hazy HgI_2 crystals (of the type tested in the present study) the values of H_K on the (1 0 0) surface at $\theta = 90$, 45 and 0° are predicted to be approximately 11, 13 and 30, respectively. (Predicted numerical values of H_K, based upon values of Ω that are at or near zero, are less reliable (quantitatively) owing to uncertainties in the effects of indentor geometry and possible slip on other hard-glide systems, although theory clearly predicts H_K to increase as Ω decreases.)

For the IFP loading the (1 0 1) plane, both type 3 slip systems are always stressed. The greatest shear stresses acting upon a type 3 slip system, as well as the maximum values of Ω, are found when the punch is aligned with the $[\bar{1}\,0\,1]$ direction. If the orientation angle is taken as 0° when the IFP is coincident with [0 1 0] and as 90° when it is aligned with $[\bar{1}\,0\,1]$, calculations of Ω based upon a CRSS of 15 yield $\Omega = 93$ at $\theta = 0°$, $\Omega = 412$ at $\theta = 90°$, and an intermediate minimum value of $\Omega = 38$ at $\theta = 20°$ (see Fig. A1). Thus, theoretically, the Knoop microhardness of the (1 0 1) surface should be lowest at $\theta = 90°$ and highest at the minimum in the Ω versus θ curve. Since $\Omega(\theta)$ passes through a rather shallow minimum at $\theta = 20°$ when the CRSS = 15, one might reasonably expect experimental H_K versus θ data to exhibit a broad maximum within the range $\theta \simeq 0$ to 45° on the (1 0 1) plane. Comparison of the values of Ω computed on the (1 0 1) plane with those on the (0 0 1) plane (for a CRSS of 15) suggests that, for indentions on the (1 0 1) plane at large values of θ (say $\theta \gtrsim 60°$), the values of H_K will be close to those on the (0 0 1) plane (particularly when θ is near 45° on the latter plane). However, for smaller values of θ (say $\theta \lesssim 45°$), H_K is expected to be substantially greater on the (1 0 1) plane than on the (0 0 1) plane. To our knowledge, Knoop microhardness measurements have not yet been made on the (1 0 0) or (1 0 1) surfaces of HgI_2. Baskar *et al.* [20] reported that the microhardness of solution-grown HgI_2 single crystals is greater on the (0 0 1) planes than on the (1 0 1) planes, by a factor of about two, when a Vickers indentor is used. This is contrary to what we would expect for Knoop microhardness on vapour-grown single crystals.

Acknowledgements

We would like to thank the UCSB Academic Senate, the State of California MICRO Program and EG&G Energy Measurements, Inc. for supporting this work. Particular thanks are due to A. Cheng, L. van den Berg, C. Ortale-Baccash and L. Franks of EG&G for supplying the crystals used in the present study and for helpful discussions.

References

1. R. W. G. WYCKOFF, "Crystal Structures", 2nd Edn, Vol. 1 (J. Wiley, New York, 1963) p. 309.
2. T. W. JAMES and F. MILSTEIN, *J. Mater. Sci.* **18** (1983) 3249.
3. P. T. RANDTKE and C. ORTALE, *IEEE Trans. Nucl. Sci.* **NS-24** (1977) 129.
4. T. W. JAMES and F. MILSTEIN, *J. Mater. Sci.* **16** (1981) 1167.
5. F. MILSTEIN, B. FARBER, K. KIM, L. van den BERG and W. F. SCHNEPPLE, *Nucl. Instr. Meth.* **213** (1983) 65.
6. S. GITS, *ibid.* **213** (1983) 43.
7. M. SCHIEBER, C. ORTALE, L. van den BERG, W. SCHNEPPLE, L. KELLER, C. N. J. WAGNER, W. YELON, F. ROSS, G. GEORGESON and F. MILSTEIN, *ibid.* **A283** (1989) 172.
8. F. MILSTEIN, T. W. JAMES and G. GEORGESON, *ibid.* **A285** (1989) 500.
9. T. W. JAMES and F. MILSTEIN, *Appl. Phys. Lett.* **52** (1988) 538.
10. P. M. PETROFF, Y. P. HU and F. MILSTEIN, *J. Appl. Phys.* **66** (1989) 2525.
11. K. JAMES, V. GERRISH, E. CROSS, J. MARKAKIS, J. MARSCHALL and F. MILSTEIN, *Nucl. Instr. Meth.* **A322** (1992) 390.
12. S. G. ROBERTS, P. D. WARREN and P. B. HIRSCH, *Mater. Sci. Eng.* **A105/106** (1988) 19.
13. G. GEORGESON and F. MILSTEIN, *Nucl. Instr. Meth.* **A285** (1989) 488.
14. J. GUILLE and M. SIESKIND, *J. Mater. Sci.* **26** (1991) 899.
15. F. MILSTEIN and G. GEORGESON, *ibid.* **24** (1989) 328.
16. S. G. ROBERTS, P. D. WARREN and P. B. HIRSCH, *J. Mater. Res.* **1** (1986) 162.
17. S. G. ROBERTS, *Phil. Mag. A* **58** (1988) 347.
18. P. B. HIRSCH, P. PIROUZ, S. G. ROBERTS and P. D. WARREN, *Phil. Mag. B* **52** (1985) 759.
19. A. NADAI, "Theory of Flow and Fracture of Solids", Vol. II (McGraw-Hill, New York, 1963) p. 217.
20. K. BASKAR, K. THANGARAJ and R. GOBINATHAN, *J. Mater. Sci. Lett.* **10** (1990) 85.

Received 13 January
and accepted 31 August 1993